Direct Observation of Melting of the Vortex Solid in $Bi_2Sr_2CaCu_2O_{8+\delta}$ Single Crystals

A. Oral, J. C. Barnard, and S. J. Bending
Department of Physics, University of Bath, Claverton Down, Bath BA2 7AY, United Kingdom

I. I. Kaya
Max Planck Institut FKF, Heisenbergstraße 1, D-70569 Stuttgart, Germany

S. Ooi and T. Tamegai
Department of Applied Physics, University of Tokyo, Bunkyo-ku, Tokyo 113, Japan

M. Henini
Department of Physics, University of Nottingham, University Park, Nottingham NG7 2RD, United Kingdom
(Received 12 December 1997)

A scanning Hall probe microscope has been used to directly observe the vortex lattice melting transition in $Bi_2Sr_2CaCu_2O_{8+\delta}$ single crystals. Below the melting line, the system settles into a fairly well-ordered vortex solid which undergoes pronounced rotations as the field is increased due to incommensurability effects. Vortex contrast is lost abruptly and discontinuously at the melting line consistent with a first order transition. Vortex profiles appear to be strongly broadened by two-dimensional fluctuations which grow much stronger as the melting line is approached from below, suggesting that melting and decoupling are almost simultaneous. [S0031-9007(98)05763-9]

PACS numbers: 74.60.Ge, 74.25.Dw, 74.72.Hs

The $Bi_2Sr_2CaCu_2O_{8+\delta}$ (BSCCO) high temperature superconductor has the strongest crystalline anisotropy of all known materials in its class leading to an extraordinarily rich magnetic field-temperature phase diagram. Controversy still surrounds some regions of this diagram, but there is broad consensus that the vortex solid melts to a liquid state at a well-defined field and temperature-dependent phase boundary. Moreover, the observation of sharp jumps in bulk magnetization [1] and local induction measurements [2] (as well as the recent corroborating calorimetric measurement of a latent heat at melting in $YBa_2Cu_3O_{7-\delta}$ [3]) suggest that it is a first order thermodynamic transition. Local induction measurements reveal that the phase boundary terminates in a multicritical point at about 40 K as the temperature is reduced. However, it has been shown recently that a continuation of the line to zero temperature can be associated with the so-called second magnetization peak, where bulk pinning is suddenly enhanced upon increasing field [4]. To date, the most compelling data on the melting line in BSCCO have come from either macroscopic measurements (e.g., bulk magnetization [1] and static Hall sensors [2]) or microscopic probes which average over a large ensemble of vortices (e.g., neutron scattering [5] and muon spin rotation [6]). Clearly, it is important to extend these studies to the truly microscopic level, where the degree of order of discrete vortices is examined as the transition line is crossed. Lorentz microscopy has been used to achieve this goal in thin ($\sim$200 nm) BSCCO films, where it was found that vortex contrast faded away close to the irreversibility line as estimated from bulk magnetization measurements [7]. Image contrast was, however, quite poor near the melting line preventing a quantitative analysis of the data, and the technique is not suitable for single crystals. We report here the first *direct* observation of melting of the vortex solid in a high quality BSCCO single crystal using a scanning Hall probe microscope (SHPM) with unprecedented field sensitivity ($\sim 3 \times 10^{-7}$ T/$\sqrt{\text{Hz}}$) and spatial resolution (~ 0.25 μm).

The basic design of our SHPM has been described in detail elsewhere [8]. In brief, a commercial low temperature scanning tunneling microscope (STM) has been modified by replacing the usual STM tip with a GaAs chip. This sensor incorporates a two-dimensional Hall probe with active area ~ 0.25 μm $\times$ 0.25 μm patterned by electron beam lithography in a GaAs/AlGaAs heterostructure positioned about 5 μm from an integrated tunneling tip at the metallized corner of an etched mesa. The sample is mounted on a stick-slip coarse approach mechanism which is used to advance it towards the sensor which is bonded directly to the end of the piezoelectric scanner tube. The sample is tilted $\sim 1^\circ$–2° with respect to the scanner plane to ensure that the STM tip is always the closest point to it. The images presented in this Letter were captured in the "flying" mode, whereby the STM tip is used to record the sample topography which can then be electronically compensated during rapid Hall probe scans with the sensor retracted ~ 0.1 μm from the crystal surface. The entire microscope assembly sits at the center of a commercial temperature-controlled cryostat incorporating a two-stage vibration isolation system.

The high quality as-grown BSCCO crystals investigated here were prepared by the traveling solvent floating zone technique [9]. The presented images were measured on

 0031-9007/98/80(16)/3610(4)$15.00

a large crystal with approximate dimensions ~3 mm × 2 mm × 100 μm while a somewhat smaller crystal from the same growth batch was investigated with a static Hall probe array in a separate cryostat with a higher field capability to generate the melting line shown in Fig. 2 (below). Both crystals have T_c of 90.5 K as estimated by a linear extrapolation of the melting line to zero field.

Once the first images had been captured, it became immediately apparent that vortex structures in BSCCO are extremely dynamic at high temperatures, and every time any single experimental parameter (e.g., H or T) was changed, the vortices took many minutes to settle into a stable configuration. This is illustrated in Fig. 1, which shows three ~7 μm × 5.6 μm quasireal time images captured near the center of the large crystal after its surface had been freshly cleaved. In this case, the sample had been zero-field cooled to 77 K after which the applied field was suddenly increased to 8 Oe and the SHPM set to repeatedly scan the same area. With the measurement bandwidth used, each scan took 45 s to complete, so there is a certain amount of movement within each frame. Nevertheless, a comparison of images 1(a)–1(c) reveals clearly substantial changes in the vortex structure which occur on the scale of minutes. As a guide to the eye, a triangular mesh has been superimposed on the data to approximately indicate the locations of the vortex centers, making it clear that successive images are distorted strongly by shear waves. In addition, vortex vacancies can be resolved clearly in the lower left corner of Fig. 1(a) and the upper right corner of Fig. 1(c) and appear to be rather mobile. After some tens of minutes, the fluctuations eventually die away leaving a reasonably well-ordered sixfold coordinated solid state. The origin of these long-term fluctuations will be discussed later in this Letter.

The position of the melting line was established from local induction measurements with the scanning Hall probe itself. The upper inset of Fig. 2 shows the magnetic induction measured for increasing applied fields at 85 K in the same location as the images were captured and note the abrupt induction increase of ~0.2 G at 23 Oe which is the accepted signature of the melting line [2]. These data were recorded with the Hall probe raised deliberately ~5 μm above the sample surface to smear away the fine structure due to discrete vortices moving under the sensor. The main graph in Fig. 2 summarizes the result of many such measurements at different temperatures (solid points). Also included are the data on the smaller crystal from the same growth batch which has been investigated to higher fields in a separate cryostat (open circles). To within the error in the field calibration of the cryostats, both sets of data agree well and conform to that measured in high quality as-grown BSCCO crystals by other authors [4]. The lower inset of Fig. 2 shows a typical SHPM image of the settled hexagonal vortex lattice after field cooling to 77 K in a field of 30 Oe. This illustrates the fact that we are not operating at the limit of our spatial resolution in the images that follow at lower applied fields.

In practice, our vortex-resolved investigations of the melting line were performed by varying the applied field at constant temperature, since any temperature variations lead to thermal drifts in the relative positions of Hall probe and sample as well as changes in the piezoelectric coefficient of the scanner tube. Our ability to resolve individual vortices near the melting line is limited by the Hall probe sensitivity and represents a tradeoff between reduced peak induction amplitudes due to vortex overlap at the higher fields required at lower temperatures and an increase in sensor noise at higher temperatures. The images in Fig. 3

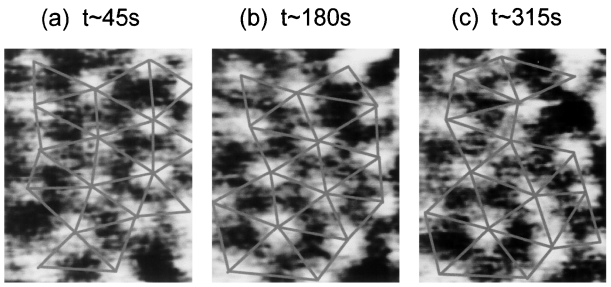

FIG. 1. Real time scanning Hall probe images (a) ~45 s, (b) ~180 s, and (c) ~315 s after the applied field is suddenly increased from zero to 8 Oe at 77 K. A triangular mesh has been superimposed to indicate the approximate location of vortex centers (image sizes ~7 μm × 5.6 μm, gray scale spans ~2.55 G).

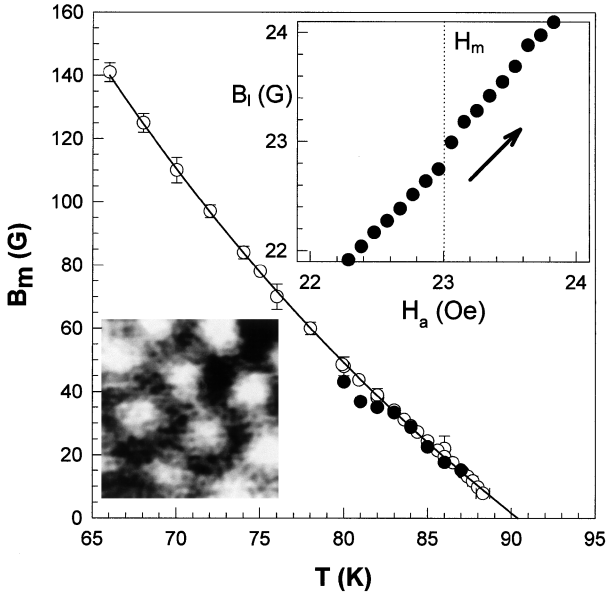

FIG. 2. The melting line measured with the SHPM on the large crystal studied (solid circles) and by a static Hall probe array on a smaller crystal from the same growth batch (open circles). Upper inset shows the measured local induction signal near the melting field for the large crystal at 85 K. Lower inset shows a typical image of the vortex lattice after field cooling to 77 K in 30 Oe (image size ~2.6 μm × 2.6 μm).

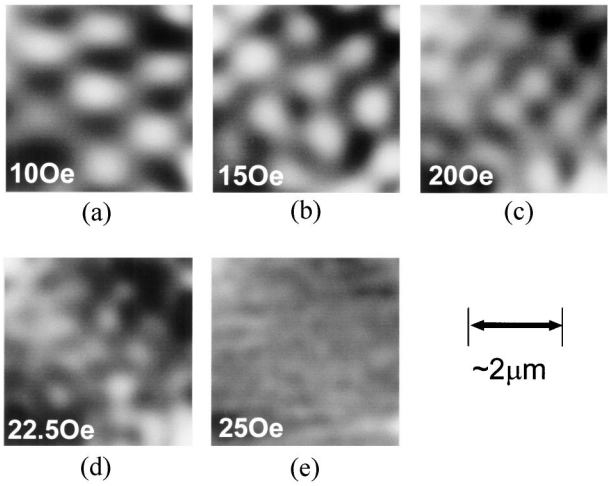

FIG. 3. Family of 85 K scanning Hall probe images at applied fields of (a) 10 Oe (gray scale spans ~0.42 G), (b) 15 Oe (~0.31 G), (c) 20 Oe (~0.21 G), (d) 22.5 Oe (~0.13 G), and (e) 25 Oe (~0.03 G) ($H_m = 23$ Oe) (image sizes ~3.8 μm × 3.8 μm).

represent points on a field cut through the melting line at 85 K ($H_m = 23$ Oe), where we have waited for an equilibrium vortex structure to stabilize in each case. To suppress some of the white noise from the Hall probe, a low pass Fourier filter has been carefully employed in these images with a cutoff spatial frequency well in excess of that expected for the vortex solid to avoid any spurious artifacts. A reasonably well-ordered sixfold symmetric structure is evident at 10, 15, and 20 Oe, and can also be identified just below the melting line at 22.5 Oe. At the melting line, vortex resolution is lost abruptly and the apparent structure in the image at 25 Oe is merely the result of low pass Fourier filtering of a white noise signal. We emphasize that we would still have ample sensitivity to resolve individual vortices above the transition line if the lattice had not melted. Fourier transforms of the images ($H < H_m$) yield six clear diffraction spots indicating good sixfold order over these relatively small regions. Careful inspection of the orientation of the vortex solid in Fig. 3 reveals pronounced rotations as the applied field is increased. Since we believe bulk pinning to be negligibly weak in this temperature regime, the vortex solid must be stabilized by a combination of a finite shear modulus and surface/geometrical barriers near the perimeter of the sample. Since the rectangular crystal and hexagonal lattice are incommensurable, the orientation of the lowest energy vortex structure will be extremely sensitive to the exact value of the applied field. Within this picture, H-dependent rotations of the vortex solid are not surprising, and we speculate that the search for this energy minimum represents the driving force for the long-term fluctuations seen wherever any external parameter is changed [cf. Figs. 1(a)–1(c)]. Images have also been generated along a cut through the melting line at 81 K and display exactly the same qualitative behavior as that shown at 85 K. The considerably larger vortex tail overlap at the higher melting field [$H_m(81\text{ K}) \cong 42$ Oe] leads, however, to greatly reduced induction peaks, and the quality of these images is much poorer, and they have not been included here.

Figure 4(a) shows typical induction line scans (offset vertically for clarity) along one of the unit vectors of the vortex solid at the five values of applied field shown in Fig. 3. Note that no Fourier filtering has been applied here, and these traces represent the raw measured data. Clearly the peak-to-valley "corrugation" along a unit vector falls rapidly as the melting line is approached. The average corrugation along various lattice vectors in the different images has been calculated and plotted against applied field in Fig. 4(b). We observe an abrupt discontinuous drop to zero at the melting field (indicated by the vertical dotted line) which is entirely consistent with the proposed first order melting transition. For comparative purposes, the corrugation predicted by the Clem variational model [10] is also plotted on this figure (solid line) assuming

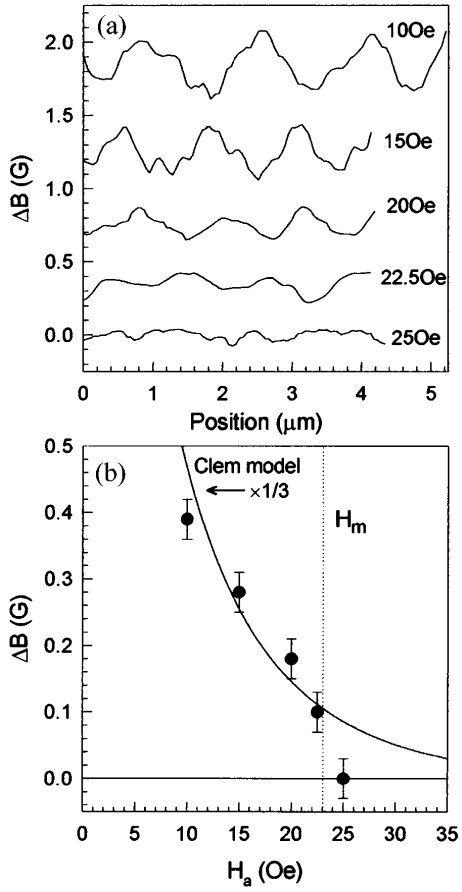

FIG. 4. (a) Typical line scans along a unit vector of the vortex lattice at various applied magnetic fields. (b) Mean vortex peak-to-valley induction corrugation along a unit vector as a function of applied field (solid points). Also shown for comparison is the corrugation predicted by the Clem model (continuous line). The position of the melting field is indicated by a vertical dotted line.

$\lambda(T) = (200\ \text{nm})\sqrt{1 - (T/T_c)^4}$ and where smearing due to the vertical separation of sample and Hall probe, and finite sensor area have been accounted for. We note that we are applying this model far out of its regime of validity, but it nevertheless illustrates two important points. The corrugation predicted by the Clem model is approximately a factor of 3 larger than the measured value indicating that the vortex profiles are very strongly fluctuation broadened at these temperatures. We also note that the model data show positive curvature as the field is raised characteristic of the increasing overlap of exponential vortex tails. This is in stark contrast to the negative curvature displayed by the measured data as the melting field is approached from below. We attribute this apparent anticipation of the melting line to increasing two-dimensional fluctuations of the vortex lines (i.e., wavier lines) which grow in amplitude as the melting field is approached, and a similar conclusion was drawn from recent muon spin rotation measurements [11]. Since such fluctuations can be viewed as the precursor to a complete breaking up of vortex lines into two-dimensional vortex pancakes, it is likely that this decoupling happens near the melting line. Whether melting and decoupling are simultaneous [12] or whether decoupling occurs at a slightly higher temperature (or field) [13] is still controversial, and the recent observation that surface barriers force transport currents to flow predominately at the edges of single crystal samples over a broad temperature range [14] has cast a shadow over these flux transformer measurements. Since we are unable to resolve any vortices above the melting field once static order has been lost, we are not in a position to make a meaningful contribution to this debate. However, we note that a quadratic extrapolation of the measured corrugation data for $H < H_m$ drops to zero at an applied field of 26 Oe. The data are not of sufficient quality to attach too much significance to this point, but we cannot rule out the possibility that vortex resolution is lost at the transition line due to the melting of strongly fluctuating vortex lines, while full decoupling takes place only at this slightly higher field.

We have previously reported pronounced low-field flux inhomogeneities in all of the high quality as-grown BSCCO crystals we have studied (including the one imaged here) [15]. At the higher fields typically encountered near the melting line, a weak modulation of the overall magnetic induction profile survives and leads to the formation of an intermediate state of coexisting vortex solid and liquid regions. The images shown in Fig. 3 have been captured in a region *between* high induction stripes and, locally, are the last parts of the vortex solid to melt as the field is increased. Consequently, our images reflect the melting of a crystallite surrounded by the liquid phase, and one would not expect them to be significantly influenced by the surrounding medium. However, images captured from the high induction stripe regions where melting occurs within a solid matrix also show the same behavior at the melting line, and we conclude that these weak flux inhomogeneities do not significantly influence the microscopic melting mechanism.

In conclusion, we have used a state-of-the-art scanning Hall probe microscope to capture high-resolution images of vortex structures as we increase the field through the melting line in as-grown BSCCO single crystals. For $H < H_m$, we observe a reasonably ordered sixfold coordinated solid, provided we wait long enough for an equilibrium state to form. The induction corrugation along the unit vectors of the solid drops abruptly and discontinuously to zero at the melting line consistent with a first order thermodynamic transition. As the melting field is approached from below, the vortex solid undergoes pronounced rotations due to the incommensurability of the hexagonal vortex solid and the rectangular surface/geometric barriers confining it. The vortex profiles appear to be broadened strongly by two-dimensional fluctuations which grow in amplitude as the melting line is approached suggesting that melting and decoupling to 2D pancakes occur along almost the same line in the H-T phase diagram.

The authors thank D. E. Farrell, M. A. Moore, N. K. Wilkin, and R. A. Doyle for useful discussions. This work was supported in the U.K. by EPSRC and MOD Grant No. GR/J03077 and the University of Bath Initiative Fund as well as a grant-in-aid for scientific research from the Ministry of Education, Science, Sports and Culture in Japan.

[1] H. Pastoriza *et al.*, Phys. Rev. Lett. **72**, 2951 (1994).
[2] E. Zeldov *et al.*, Nature (London) **375**, 373 (1995).
[3] A. Schilling, *et al.*, Nature (London) **382**, 791 (1996).
[4] B. Khaykovich *et al.*, Phys. Rev. Lett. **76**, 2555 (1996).
[5] R. Cubitt *et al.*, Nature (London) **365**, 407 (1993).
[6] S. L. Lee *et al.*, Phys. Rev. Lett. **71**, 3862 (1993).
[7] K. Harada *et al.*, Phys. Rev. Lett. **71**, 3371 (1993).
[8] A. Oral, S. J. Bending, and M. Henini, Appl. Phys. Lett. **69**, 1324 (1996).
[9] N. Motohira *et al.*, J. Ceram. Soc. Jpn. **97**, 994 (1989).
[10] J. R. Clem, in *Proceedings of the 14th International Conference on Low Temperature Physics*, edited by M. Krusius and M. Vuorio (North-Holland, Amsterdam, 1975), Vol. 2, p. 285.
[11] S. L. Lee *et al.*, Phys. Rev. Lett. **75**, 922 (1995).
[12] D. T. Fuchs *et al.*, Phys. Rev. B **55**, R6156 (1997).
[13] C. D. Keener *et al.*, Phys. Rev. Lett. **78**, 1118 (1997).
[14] D. T. Fuchs, E. Zeldov, M. Rappaport, T. Tamegai, and S. Ooi (to be published).
[15] A. Oral *et al.*, Phys. Rev. B **56**, R14 295 (1997).